eal and virtual bremsstrahlung in few-body systems

celar, JCS

blished in:
a Physica Polonica B

blication date:
02

REAL AND VIRTUAL BREMSSTRAHLUNG IN FEW-BODY SYSTEMS*

J.C.S. Bacelar

Kernfysisch Versneller Instituut
Zernikelaan 25, 9747AA Groningen, the Netherlands

(Received February 7, 2002)

The real- and virtual-photon emission during interactions between few-nucleon systems have been investigated at KVI with a 190 MeV proton beam. Here I will concentrate the discussion on the results of the virtual-photon emission for the proton–proton system and proton–deuteron capture. Predictions of a fully-relativistic microscopic-model of the proton–proton interaction are discussed. For the proton–deuteron capture process the data are compared with predictions of a relativistic gauge-invariant impulse approximation and a Faddeev calculation. For the virtual photon processes, the nucleonic electromagnetic response functions were obtained for the first time and are compared to model predictions.

PACS numbers: 25.20.Lj

1. Introduction

The study of photon emission during nucleon–nucleon collisions provides a sensitive and unobtrusive way to study the nucleon–nucleon interaction. The photon couples directly to the electromagnetic currents associated with the dynamics of the collision. Recent accurate measurements [1, 2] of this process provided exciting developments [3–6] in the theoretical attempts to describe the interacting nucleons. Most of the precise data are associated with proton–proton collisions, for obvious experimental simplicities.

At KVI we have performed [2] the most accurate measurements to date on the reaction $pp \to pp\gamma$. Here I discuss the virtual-bremsstrahlung, $pp \to ppe^+e^-$, yields [7, 8]. The proton beam is polarized, with the energy of 190 MeV. A liquid H_2 target is used to reduce background. The forward angle hodoscope SALAD (Small Angle Large Acceptance Detector) was used to measure the energies and the tracks of the two protons, within scattering

* Presented at the VI TAPS Workshop, Krzyże, Poland, September 9–13, 2001.

polar angles of 6° and 28°. It consists of two wire chambers (with a total of five wire planes) and two stacked planes of scintillator detectors (see Fig. 1). This detector is equipped with a specially designed trigger system which allows it to deal with the unwanted 14 MHz rate of the elastic channel at these small angles. The virtual photon was detected with TAPS, an array of 384 BaF_2 crystals which for the data discussed here were placed in the median plane around the target in blocks of 8×8 crystals. The experimental setup shown in this figure is common to all the experiments discussed in this paper.

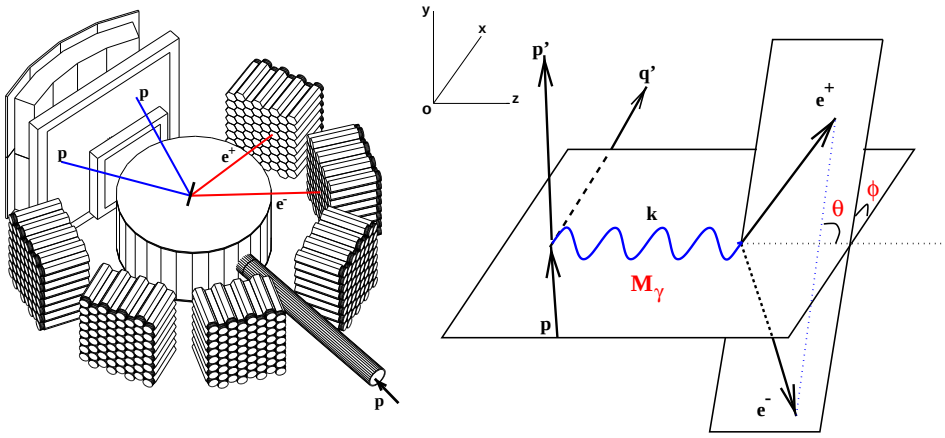

Fig. 1. Left: Schematic view of the experimental setup consisting of SALAD (two wire-chambers and 50 plastic scintillators) and TAPS (384 hexagonal BaF_2 crystals). Not drawn are the thin plastic scintillators placed in front of each BaF_2 crystal. An example of a ppe^+e^- event originating from the liquid-hydrogen target is indicated. On the right panel the chosen coordinate system to describe the dynamics of these events is given.

2. Proton–proton bremsstrahlung

During this experiment we measured [7,8] for the first time the virtual-photon emission process, which in the laboratory means the measurement of the positron–electron pair. Such an event is shown in Fig. 1. The added information provided by the virtual photon is the decomposition of the electromagnetic response of the nucleon in components related to the polarizations of the photon. The six nucleonic response functions are related to specific angular distributions of the two leptons. Following reference [9] the reaction cross section for the virtual bremsstrahlung process, $pp \to ppe^+e^-$,

is proportional to the following amplitude:

$$
\begin{aligned}
|A|^2 \;=\; & \frac{1}{M_\gamma^2}\Bigg\{ W_T\left(1-\frac{\ell^2}{2M_\gamma^2}\sin^2\theta\right) + W_L\left(1-\frac{\ell^2}{k_0^2}\cos^2\theta\right) \\
& + \frac{\ell^2\sin^2\theta}{2M_\gamma^2}\left(W_{\mathrm{TT}}\cos 2\phi + W'_{\mathrm{TT}}\sin 2\phi\right) \\
& + \frac{\ell^2\sin 2\theta}{2k_0 M_\gamma}\left(W_{\mathrm{LT}}\cos\phi + W'_{\mathrm{LT}}\sin\phi\right)\Bigg\}, \qquad (1)
\end{aligned}
$$

where M_γ and k_0 are the invariant mass and the energy of the virtual photon, respectively. The polar (θ) and azimuthal (ϕ) angles of the momentum-difference vector, ℓ, of the two leptons are shown in Fig. 1. The cross-section for the virtual bremsstrahlung process as a function of the invariant mass of the photon, as well as its angular distribution are plotted in Fig. 2.

The data are compared with predictions of the fully-relativistic microscopic-calculation [6] (solid line) as well as a low energy (LET) calculation [9, 10] (dashed line). The microscopic-model, based on the Fleischer–Tjon potential [11], includes the off-shell dynamics of the interacting protons. It includes virtual Δ-isobar excitations, meson exchange currents, negative energy states and rescattering diagrams explicitly. The LET calculation uses an expansion procedure for the on-shell T-matrix in order to account for the off-shell dynamics of the interacting protons. Furthermore, it takes into account only the rescattering contributions, meson-exchange currents and the virtual Δ-isobar excitation by enforcing charge and current conservation. The microscopic calculation overpredicts the virtual photon data by approximatelly 30% over the full acceptance of the experimental setup. The LET calculation on the other hand reproduces the data rather well. We note that the cross-section depicted in Fig. 2, is integrated over the leptonic angles and is therefore a measure of the transverse (W_{T}) and longitudinal (W_{L}) nucleonic response functions. The interference terms cancel out in the integration over the leptonic phase-space (see equation (1)). A similar discrepancy was observed for the real photon differential cross-sections. In many regions of the phase space, the microscopic model overpredicts the data, whereas the LET calculation is, in all regions of the phase space covered in the experiment, in excellent agreement with the data. We note that whereas the LET calculations use a proton–proton potential which is fitted to the worlds elastic data (phase-shifts), the microscopic model uses a Fleischer–Tjon relativistic potential which does not describe the elastic data with the same degree of precision. Work is at the moment in progress to fit this potential to the worlds proton–proton elastic data. The different amplitudes of the orthogonal cosine and sine functions of the leptonic dihedral

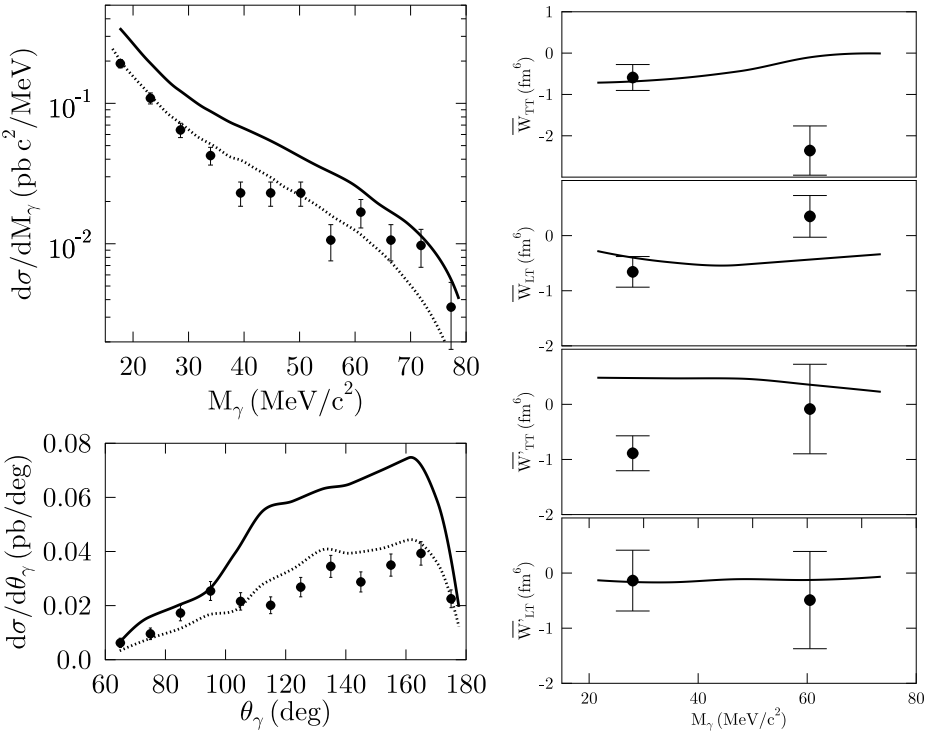

Fig. 2. Top left: differential cross section as a function of the invariant mass (M_γ) of the virtual photon integrated over the entire detector acceptance. Bottom left: virtual-photon angular distribution in the laboratory frame for invariant masses integrated from 15 to 80 MeV/c^2. Right: The experimental values of the proton electromagnetic interference response functions $\overline{W}_{\rm TT}$, $\overline{W}_{\rm LT}$, $\overline{W'}_{\rm TT}$ and $\overline{W'}_{\rm LT}$. The solid lines present the results of a microscopic model and the dotted lines the results of a LET calculation.

angle ϕ (see Fig. 1 and equation (1)) were extracted from the data. They are directly related to each of the four interference nucleonic response functions: $W_{\rm TT}$, $W_{\rm TL}$, $W'_{\rm TT}$ and $W'_{\rm TL}$. The experimentally extracted response functions are shown in Fig. 2. They are integrated over the full acceptance of our experimental setup, and shown for two regions of the invariant mass of the photon. The predictions of the fully relativistic calculations are also shown as solid lines. Within the accuracy of the data the model predictions are in general good. These response functions are sensitive to the different diagrams included in the calculations, and with an accurate dataset one will be able to disentangle the effects of individual diagrams.

3. Proton–deuteron capture process

Another reaction investigated was proton-deuteron scattering. All exit channels were measured. Here I will only discuss the process $pd \rightarrow {}^3\mathrm{He}$ both for real as well as virtual photon capture [12]. The experimental setup is the same as in the proton-proton studies. The experiment was performed with an integrated luminosity of 370 ± 40 pb^{-1}. We have identified 12000 real-photon capture events and 300 events from the $pd \rightarrow {}^3\mathrm{He}{+}e^+e^-$ reaction. Only events with invariant mass $M_\gamma > 15$ MeV were selected [7,8].

The differential cross-sections as function of the photon angle are shown for the real and virtual photon capture in Fig. 3. For the real photon capture our data are compared with previously published data from IUCF [13] measured at a proton beam energy of 150 MeV, and an experiment performed at

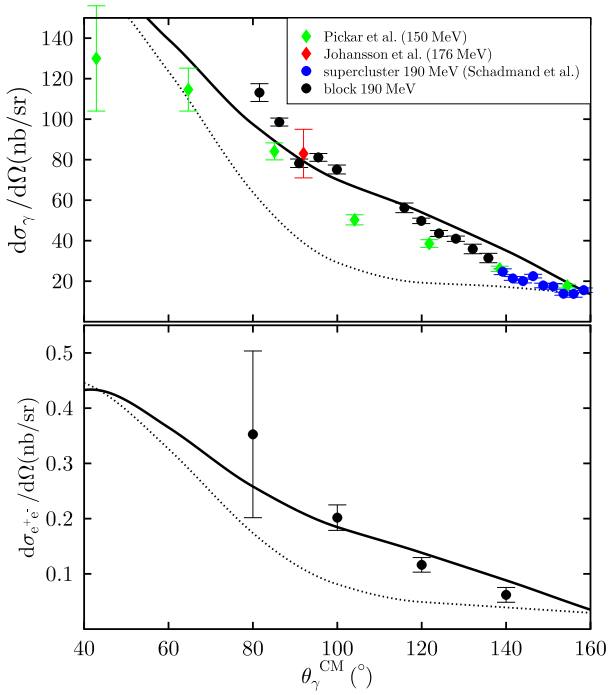

Fig. 3. The real- (top) and virtual-photon (bottom) capture cross sections of the $pd \rightarrow {}^3\mathrm{He}{+}\gamma^{(*)}$ reaction as a function of $\theta_\gamma^{\mathrm{CM}}$. Present data are shown as full dots. Empty dots, and full and empty diamonds are data from Refs. [5,6] and [7], respectively. The lines are the results of calculations using a relativistic gauge-invariant model (solid and dotted curves) as discussed in the text. For the virtual-photon case the data and calculations are integrated for $M_\gamma > 15$ MeV.

TSL [14] at 176 MeV. Furthermore, the data are compared to calculations with a relativistic gauge-invariant model [15] (dotted curve) and a recent Faddeev calculation [16] (not shown). The latter includes initial-state interactions as well as π and ρ meson exchange currents explicitly, with the method outlined in Ref. [17]. The solid lines are discussed below.

In the impulse approximation, radiation from all external legs are included, and a contact term, constructed by applying gauge-invariance, is used to account for other contributions such as meson-exchange currents, *etc.*

The discrepancy noted for the real-photon capture cross section is also observed for the virtual-photon capture process in the angular range $70^\circ < \theta_\gamma^{\rm CM} < 140^\circ$ (see dotted lines in figure 3).

In an attempt at fitting the real-photon cross sections, Ref. [18] introduces an *ad-hoc* parameter (α) which enhances the magnetic contribution. Calculations of this model with $\alpha = 1.2$ are shown as solid lines in Fig. 3. This value of α is chosen such that it best fits the real-photon capture cross sections at 190 MeV. The large discrepancy between theoretical predictions and experimental data for both the real- and virtual-photon capture cross sections implies enhanced transverse radiation which could be attributed to magnetic contributions. An example of such a process is the virtual excitation of the Δ. This process is not taken into account in the theoretical predictions shown as dotted lines in Fig. 3, and also not in the Faddeev calculations [16].

4. Future plans at KVI

At KVI this whole program is going to enter its second phase, whereby the Plastic Ball detector [19], originally developed at GSI, is used as a photon/dilepton spectrometer. This detector has an almost complete coverage of 4π for the electromagnetic radiation, and increases the efficiency of the experiments reported here by a factor of 25. It is highly granular, with a total of 654 phoswich elements. At KVI this detector has been modified (see Fig. 4) to operate with a liquid H_2 target. Furthermore, modifications are underway to include an inner-shell of Cherenkov-detectors which will provide a highly selective trigger for dilepton events. The electromagnetic response functions of the proton will be studied with a precision such that the effects of different diagrams entering in the nucleon–nucleon interaction can be disentangled.

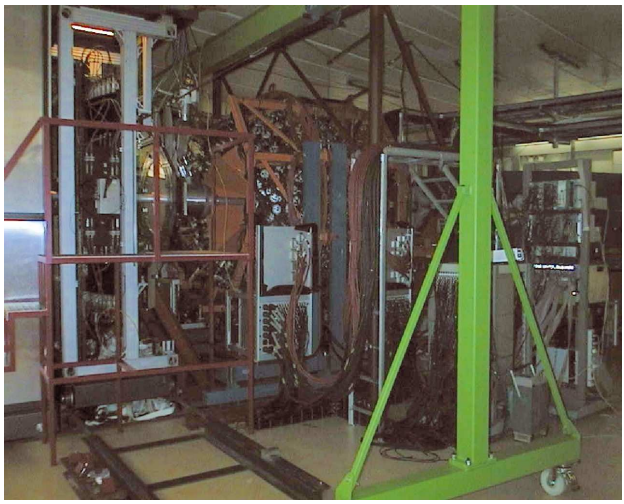

Fig. 4. The Plastic Ball and SALAD detectors at KVI.

I would like to acknowledge all my KVI collaborators: M.J. van Goethem, M.N. Harakeh, M. Hoefman, H. Huisman, N. Kalantar-Nayestanaki, H. Löhner, J.G. Messchendorp, R. Ostendorf, S. Schadmand, R. Turissi, M. Volkerts, H.W. Wilschut, A. van der Woude, and the TAPS Collaboration. This work was supported in part by the "Stichting voor Fundamenteel Onderzoek der Materie" (FOM) with financial support from the "Nederlandse Organisatie voor Wetenschappelijk Onderzoek" (NWO), by GSI, the German BMBF, and by the European Union HCM network under contract HRXCT94066.

REFERENCES

[1] K. Michaelian *et al.*, *Phys. Rev.* **D41**, 2689 (1990).
[2] H. Huisman *et al.*, *Phys. Rev. Lett.* **83**, 4017 (1999).
[3] F. de Jong, K. Nakayama, *Phys. Lett.* **B385**, 33 (1996).
[4] J.A. Eden, M.F. Gari, *Phys. Rev.* **C53**, 1102 (1996).
[5] G.H. Martinus, O. Scholten, J.A. Tjon, *Phys. Rev.* **C58**, 686 (1998).
[6] G.H. Martinus, O. Scholten, J.A. Tjon, *Few-Body-Syst.* **26**, 197 (1999).
[7] J.G. Messchendorp *et al.*, *Phys. Rev.* **C61**, 064007 (2000).
[8] J.G. Messchendorp *et al.*, *Phys. Rev. Lett.* **82**, 2649 (1999); *Phys. Rev. Lett.* **83**, 2530 (1999).
[9] A.Yu. Korchin, O. Scholten, *Nucl. Phys.* **A581**, 493 (1995).
[10] A.Yu. Korchin, O. Scholten, D. Van Neck, *Nucl. Phys.* **A602**, 423 (1996).

[11] J. Fleischer, J.A. Tjon, *Nucl. Phys.* **B84**, 375 (1975); *Phys. Rev.* **D21**, 87 (1980).

[12] J.G. Messchendorp *et al.*, *Phys. Lett.* **B481**, 171 (2000).

[13] M.J. Pickar *et al.*, *Phys. Rev.* **C35**, 37 (1987).

[14] R. Johansson *et al.*, *Nucl. Phys.* **A641**, 389 (1998).

[15] A.Yu. Korchin *et al.*, *Phys. Lett.* **B441**, 17 (1998).

[16] J. Golak, private communication; and W. Glöckle *et al.*, *Phys. Rep.* **274**, 107 (1996).

[17] R. Schiavilla *et al.*, *Phys. Rev.* **C40**, 2294 (1989).

[18] A.Yu. Korchin, O. Scholten, *Phys. Rev.* **C59**, 1890 (1999).

[19] A. Baden *et al.*, *Nucl. Instrum. Methods Phys. Res.* **203**, 189 (1982).